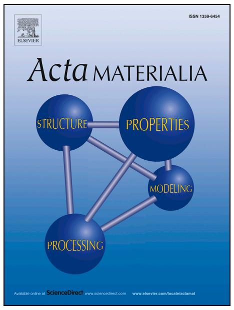

Tuning the magnetic properties of pure hafnium by high pressure torsion

C.M. Cepeda-Jiménez, J.I. Beltrán, A. Hernando, M.A. García, F. Ynduráin, A. Zhilyaev, M.T. Pérez-Prado

PII: S1359-6454(16)30819-9
DOI: 10.1016/j.actamat.2016.10.052
Reference: AM 13294

To appear in: *Acta Materialia*

Received Date: 22 July 2016
Revised Date: 20 October 2016
Accepted Date: 21 October 2016

Please cite this article as: C.M. Cepeda-Jiménez, J.I. Beltrán, A. Hernando, M.A. García, F. Ynduráin, A. Zhilyaev, M.T. Pérez-Prado, Tuning the magnetic properties of pure hafnium by high pressure torsion, *Acta Materialia* (2016), doi: 10.1016/j.actamat.2016.10.052.

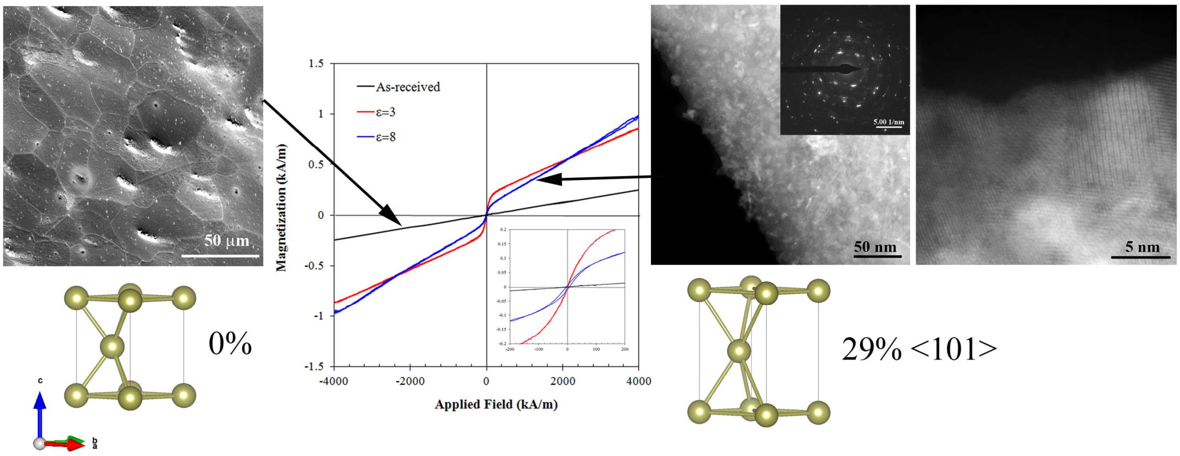
50 μm
0%
c
b
a
1.5
1
0.5
0
-0.5
-1
-1.5
Magnetization (kA/m)
As-received
ε=3
ε=8
-4000
-2000
0
2000
4000
Applied Field (kA/m)
5.00 1/nm
50 nm
5 nm
29% <101>

Tuning the magnetic properties of pure hafnium by high pressure torsion

C.M. Cepeda-Jiménez[1], J.I. Beltrán[1], A. Hernando[2,3], M.A. García[2,4], F. Ynduráin[5,6], A. Zhilyaev[7,8], M.T. Pérez-Prado[1,*]

[1]IMDEA Materials Institute, C/ Eric Kandel, 2, 28906 Getafe, Madrid, Spain
[2]Instituto de Magnetismo "Salvador Velayos", UCM, ADIF, CSIC, Las Rozas, P.O. Box 155, 28230 Madrid, Spain
[3]Departamento de Física de Materiales, Universidad Complutense, 28040 Madrid, Spain
[4]Instituto de Cerámica y Vidrio, CSIC, Cantoblanco, 28049 Madrid, Spain
[5]Departamento de Física de la Materia Condensada, Universidad Autónoma, 28049 Madrid, Spain
[6]Condensed Matter Physics Center (IFIMAC), Universidad Autónoma, 28049 Madrid, Spain
[7]Fundació CTM Centre Tecnològic, 08243 Manresa, Barcelona, Spain
[8]Institute for Metals Superplasticity Problems, 450001 Ufa, Russia

[*]Corresponding author: teresa.perez.prado@imdea.org (+34 915493422/1038)

Abstract

This work demonstrates that room temperature (RT) ferromagnetism might be triggered in pure hafnium (Hf), a classic paramagnet, by severe plastic deformation (SPD) via high pressure torsion (HPT). The origin of this phenomenon is elucidated by a combined approach including density functional theory (DFT) calculations and transmission electron microscopy (TEM). In particular, it is shown that the elastic lattice distorsions induced in pure Hf as a consequence of grain refinement down to the nanocrystalline regime by HPT lead to the development of a new monoclinic crystalline structure that exhibits a spontaneous magnetization at RT. DFT calculations are utilized to prove that local stretching of the original pure Hf hexagonal close packed (hcp) lattice along specific pyramidal directions, due to the presence of internal stresses in the deformed nanostructure, may give rise to the emergence of the monoclinic phase, which is endowed with a net magnetic moment. An excellent agreement is found between DFT calculations and experimental TEM observations, which provide a first evidence of the presence of the pure Hf monoclinic crystal lattice. This work shows that SPD may constitute a viable, yet widely unexplored, strategy to tune the magnetic properties and, in particular, to induce RT ferromagnetism in bulk non-magnetic metals.

Keywords: Monoclinic hafnium, room temperature ferromagnetism, density functional theory, internal stresses, plastic deformation.

1. Introduction

Room temperature ferromagnets are critical to a wide range of applications in key industrial sectors including energy generation and storage, electronics, biomedicine, and transport [1]. The emergence of spontaneous spin ordering in metals is achieved, according to the Stoner criterion [2,3], when the product of the density of states at the Fermi level, $N(E_F)$, and the exchange interaction, J, is greater than 1. Unfortunately, only a handful of pure metallic materials (Fe, Co, Ni, Gd) exhibit room temperature ferromagnetism [4,5]. The vast majority of metals are considered non-magnetic (paramagnetic or diamagnetic) since, although they can be weakly magnetized in the presence of an external field, their magnetization vanishes once the field is withdrawn [6].

Attempts to trigger ferromagnetism in diamagnetic and paramagnetic metals and alloys without altering their chemical composition must devise alternative ways to modify permanently their electronic properties. This has been accomplished only in a few cases and mostly at a local scale. Sampedro et al. [7] have reported RT ferromagnetism in 2.4 nm size twinned Pd nanoparticles, a phenomenon that was attributed to lattice distortions in the vicinity of the twin boundaries. Similarly, Crespo et al. [8] observed RT ferromagnetism in thiol capped 1.2 nm size Au nanoparticles due to the presence of 5d localized holes generated through Au-S bonds. Finally, Al Ma´Mari et al. [9] have demonstrated that it is possible to overcome the Stoner criterion at RT in 2 nm thick copper films interfaced with C_{60} molecular layers. It has recently been shown that bulk RT ferromagnetic behaviour may be induced in paramagnetic metals such as titanium, zirconium and magnesium by straining [10]. The origin of this phenomenon remains, however, widely unknown.

Elastic strain engineering (ESE) has been recently put forward as an efficient method to design materials with unprecedented properties [11]. This methodology exploits the fact that nanostructured materials such as thin films, nanowires, nanoparticles, bulk nanocomposites, and atomic sheets can withstand anomalously high non-hydrostatic (e.g., tensile or shear) stresses, and are thus able to sustain much larger elastic strains than in bulk, coarse grained, form. The dramatic alterations of the elastically strained crystal structures with respect to their relaxed counterparts lead to the emergence of unique functional properties. For example, it has recently been shown that inhomogenous elastic strain can be utilized to tune the bandgap of an initially homogenous monolayer membrane of MoS_2, allowing it to capture a broader range of the solar spectrum, and thus increasing its potential for photovoltaic devices [12,13]. It has also been demonstrated by first-principles calculations that ESE can be a very useful tool to control the bandgap and, thus, the electronic and optical properties of zigzag BN nanoribbons [14], thus increasing their applicability in electronic, piezoelectric, photovoltaic, and opto-electronic devices. Furthermore, elastic strain can also be utilized to enhance the properties of known ferroic oxides, to convert oxides that are neither ferroelectric nor ferromagnetic in their unstrained state into ferroelectrics, ferromagnets or multiferroic materials, or to create new tunable microwave dielectrics with outstanding performance [15]. Strain has also been widely utilized with great commercial success in Si technology to enhance the carrier mobility [16], as well as to boost the chemical reactivity and the electrocatalytic properties of metal and oxide surfaces [17], or to alter the lattice parameter and, thus, the electronic states, of semiconductor nanowires [18]. Finally, it has recently been shown [19] that, under an applied load which leads to elastic strains slightly larger than 5%, it is possible to increase the superconducting transition temperature and the critical magnetic field of kilogram scale Nb nanowires embedded in a metallic matrix. The potential of ESE to design materials with singular functional properties is still largely unexplored. In particular, to date, no studies have applied this methodology to tune the magnetic behavior of metals.

Pure Hafnium is a transition metal belonging to Group IV of the periodic table. Under equilibrium conditions it exhibits an hcp lattice (α) at 100 kPa (1 atm) and 298 K. This phase undergoes a wide range of solid state phase transformations when subjected to high temperatures and high pressures [20]. In particular, upon heating, hcp Hf transforms into a body centred cubic (bcc) structure (β) at 2016 K before reaching the melting temperature. With increasing isostatic pressure, at RT, hcp Hf transforms into a simple hexagonal lattice (ω) at 30-35 GPa and into a bcc lattice at 70 GPa [21]. Recent work [22] has shown that a face centred cubic (fcc) form of pure Hf can be stabilized by high energy milling of powders. This was accompanied by a lattice expansion of about

6%. To our knowledge, no other pure Hf crystalline structures have been reported so far.

This paper reports how pure hcp Hf can be partially transformed by severe straining into a monoclinic phase that exhibits RT ferromagnetic behavior. Several samples of the original, coarse grained, material, were processed at RT by HPT using a pressure of 6 GPa and 5 anvil turns. The resulting nanostructures, which are shown to exhibit a ferromagnetic component, are exhaustively characterized by TEM. DFT calculations are then utilized to gain further insight about the source of the emerging ferromagnetism, which is found to be originated by the elastic strains induced in the nanocrystalline processed pure Hf as a consequence of the high density of interfaces. This work provides solid evidence of the possibility of tuning the magnetic behaviour of metals by severe straining.

2. Experimental procedure

Polycrystalline pure Hf (99.7% purity, Table 1) was purchased in the form of a 10 mm diameter round bar. Disks with a thickness of 1 mm were sliced out of the as-received bar and were then severely strained at 298 K by high pressure torsion (HPT) [23]. An unconstrained setup, consisting of a bottom anvil with a flat surface, where the sample is placed, and a top anvil that exerts a pressure on the specimen and, subsequently, rotates a predetermined number of turns, was utilized. A pressure of 6 GPa and 5 full rotations of the anvil (at an approximate speed of 1 rotation per minute) were applied. The final thickness of the deformed samples was approximately 0.2 mm. The equivalent true strain imposed (ε), which is a function of the disk radius (r), is given by the following equation [22]:

$$\varepsilon = ln\left(\frac{2\pi N\cdot r\cdot h_0}{h^2}\right) \tag{1}$$

where h_0 and h are, respectively, the initial and final thicknesses of the disk, and N denotes de number of anvil turns.

The magnetization curves of the as-received and deformed pure Hf were measured between RT and 5 K using a Physical Property Measurement System vibrating sample magnetometer (PPMS-VSM) and a Magnetic Property Measurement System (MPMS-SQUID), both from Quantum Design, with a maximum field of 5 T. Measurements of the magnetic behavior were carried out in 3 mm-diameter and 200 μm-thick foils punched out of the disks processed by HPT. In particular, the center of the foils was approximately located, respectively, at r values of 0.025 mm and 3.5 mm. At these points, according to equation (1), the corresponding true strains are, respectively, ~3 and ~8. These foils were subsequently annealed at 1273 K for 5 h and their RT magnetization curves were also measured.

The microstructure of the as-received and annealed samples was examined by scanning electron microscopy (SEM) and electron backscatter diffraction (EBSD) using a field emission gun SEM (Helios NanoLab 600i, FEI) equipped with an HKL EBSD system, a CCD camera and the Channel 5.0 data acquisition and analysis software package. EBSD measurements were conducted at an accelerating voltage of 15 kV and 2.7 nA. The average grain size values were calculated by the linear intercept method from SEM and EBSD maps in the normal direction to the disk surfaces. Sample preparation for EBSD included mechanical mirror-polish using first diamond pastes of increasingly finer particle sizes and then a colloidal silica slurry finishing. Final surface finishing was carried out by electropolishing using a solution of 90% perchloric acid and 10% acetic acid and a voltage of 20 V. The nanostructure of the deformed specimens was analyzed by transmission electron microscopy using a 200 kV Talos

F200X (FEI) microscope. With that purpose, the foils that were utilized for magnetic characterization, corresponding to strains of ~3 and ~8, were mechanically thinned to about 100 μm followed by electrochemical polishing to electron transparency at RT in a Struers Tenupol-5 double-jet twin electropolisher using a solution of 90% perchloric acid and 10% acetic acid and a voltage of 20 V. Selected area electron diffraction (SAED) patterns were acquired in the as-received and deformed pure Hf in order to identify the phases present.

Ab-initio methods were utilized to investigate the effect of lattice straining on the bulk magnetic moment. DFT calculations were performed using the Perdew, Burke and Ernzerhof (PBE) approximation [24] for the exchange-correlation functional and the projector augmented plane wave method as implemented in the Vienna ab-initio Simulation Package (VASP) [25-27]. Pseudopotentials were utilized for the description of the Hf core electrons while the $5d^3$ $6s^1$ electrons were treated quantum mechanically. Full relaxation of the atomic positions and cell vectors (keeping hexagonal symmetry) was performed till the atomic forces were below 0.01 eV/Å obtaining lattice parameters a=3.192 and c=5.042 Å. These values match well with the experimentally measured values (a=3.196 and c=5.051 Å) [28]. The employed kinetic energy cutoff is 225 eV but convergence tests were performed up to 300 eV, obtaining similar values. The energy tolerance parameter utilized is 10^{-6} eV and the k-point meshes used for the electronic convergence and density of state calculations are 11x11x7 and 14x14x9, respectively, in the Monkhorst-Pack scheme [29]. The results were further validated after performing additional calculations with a 22x22x14 k-point mesh and a localized orbitals´ code (SIESTA) [30].

3. Results and discussion

Figure 1 consists of an SEM (Fig. 1a) and a TEM (Fig. 1b) micrograph illustrating the coarse-grained microstructure of the as-received pure Hf. It consists of equiaxed grains, of about 40 μm in size, with an intragranular dislocation density of approximately $3x10^{12}$ m^{-2}. Severe refinement down to the nanocrystalline range takes place during HPT processing. Fig. 2 illustrates the nanostructure developed in the samples deformed up to ε~3 (Fig.2a) and ε~8 (Fig.2b) as well as the corresponding SAED pattern. While grains with diameters ranging from 20 to 50 nm can be distinguished in both cases, the image also contains areas with no grain contrast, suggesting that the structure in those areas is finer than the thickness traversed by the electron beam. Fig. 3a is a higher magnification STEM image of a very thin area located near the rim of the centre hole of the TEM specimen which was strained up to ε~8, where, indeed, a large population of grains with sizes ranging from 5 to 20 nm can be clearly noticed. In particular, a significant fraction of grains have diameters smaller than 10 nm, as evidenced in the high resolution TEM image of Fig. 3b. The SAED pattern corresponding to this region, formed by relatively wide spots and where well defined rings are absent, evidence the present of significant lattice distortions within the finest grains. Previous works dealing with high pressure torsion of pure Hf [31] have reported grain sizes ranging from 50 nm to 400 nm following processing using pressures as high as 30 MPa and up to 10 anvil turns. We believe that the presence of such fine grains has in general been overlooked because they are only detectable by TEM in areas that are very close to the rim of the centre hole of TEM specimens, where the thickness traversed by the electrons is comparable to the grain size.

Fig. 4a compares the RT magnetization curves corresponding to the pure Hf under investigation in the as-received condition and severely deformed up to true strains of ε~3 and ε~8. It can be clearly seen that, while the as-received material exhibits the expected paramagnetic behavior, with a susceptibility (χ) of 0.634×10^{-4}, the strained specimens present an additional ferromagnetic component, as well as higher χ values. Subtle differences can be observed between the magnetic responses of the two deformed samples. More specifically, increasing the strain results in a lower saturation magnetization (M_s), higher coercive field (H_c) and higher χ. In particular, for ε~3, M_s=0.199 KA/m, H_c=1990 A/m, and $\chi=2.27\cdot 10^{-4}$; for ε~8, M_s=0.066 KA/m, H_c=14328 A/m, and $\chi=1.632\cdot 10^{-4}$. Fig. 4b compares the variation with temperature of the magnetization in the as-received state and following straining up to ε~8 at an applied field of 1 T. For the as-received sample, the temperature dependence of the magnetization reveals the existence of two components: one that decreases with T and follows the Curie law and another that is independent of temperature and corresponds to Pauli paramagnetism. The heavily deformed sample exhibits a similar trend, with larger Pauli paramagnetism. The thermal dependence of the magnetization for this sample results more complicated to analyze since both the ferromagnetic and Curie paramagnetic components decrease with temperature.

The origin of the observed RT spontaneous magnetization is now elucidated. It must be first clarified that it cannot be attributed to an increase in the Fe content in the deformed samples due to contamination from the steel anvils. The chemical compositions of pure Hf in the as-received state and deformed up to ε~8, measured by inductively coupled plasma spectroscopy (ICP-OES), are compared in Table 1. The increment in the amount of Fe impurities during processing is, indeed, very small.

Moreover, the crossover of the magnetization curves corresponding to the two deformed samples at an applied field of approximately 3 T confirms that the observed increase in M_s can not be attributed to the presence of impurities as, in that case, the magnetization curve of the sample strained up to $\varepsilon \sim 3$ should exhibit higher M values in the entire range of applied field values investigated.

The emergence of RT ferromagnetic behaviour must, thus, be originated by the changes in the density of states (DOS) due to the microstructural changes that take place upon straining and, in particular, by the formation of a nanocrystalline structure. It is well known that severe elastic lattice distortions are inherent to nanocrystalline materials. On the one hand, grain boundaries and triple junctions, with different degrees of disorder, locally modify the atomic structure by reducing the atomic density and by altering the coordination between nearest-neighbor atoms with respect to the perfect crystal [32]. Since the volume fraction of intercrystalline regions in nanomaterials is very large (approximately 50% in a polycrystal with an average grain size of 5 nm [33]), such regions often have a dramatic influence on the properties [34-38]. A second source of lattice distortions are the internal stresses resulting from the need to accommodate the strain imposed during processing between neighboring grains, which may lead to significant elastic strains. Both the magnitude and the grain-to-grain variance of such stresses increase dramatically when the grain size decreases below 15 nm [39]. Moreover, for such fine nanocrystals, internal stresses might span a large portion of the grain interiors, leading to wide variations in the lattice parameters [40,41] and, thus, potentially, in the symmetry associated with different grains. In particular, nanomaterials undergoing severe plastic deformation tend to exhibit expanded lattices, especially when the average grain size lies below ≈25 nm [40]. It is our contention that the elastic lattice distortions associated with the very fine pure Hf nanostructure developed during HPT straining lead to the emergence of the reported RT spontaneous magnetization.

Ab-initio DFT calculations (Fig.5) confirm that a net magnetic moment appears when the original pure Hf hcp lattice is stretched up to 40% along five crystallographic directions. Fig. 5 illustrates how spin moments close to 1 Bohr magneton ($\mu_{B,}$ $1\mu_B$=9.274x10^{-24} JT^{-1}) per atom in magnitude emerge from stretching along some pyramidal directions, a process that leads to a transition to a monoclinic lattice. For example, a spin moment close to 0.85 μ_B per atom results from a 29% stretch along the <101> direction and from a 40% stretch along the <102> and <201> directions. The pyramidal direction <101> is the most relevant since non-negligible spin moments appear already after a stretch of 19%. The original hcp lattice and the simple monoclinic lattices resulting from stretching 20% and 29% along the <101> direction are also plotted in Fig. 5. The corresponding lattice parameters are, for the 20% stretch configuration, a= 3.86157 Å; b/a ratio=1.58; c/a ratio=1.740724; cos (β)=-0.91156, and, for the 29% stretch configuration, a= 4.11688 Å; b/a ratio=1.58; c/a ratio=1.746578; cos (β)=-0.92318. Stretching along basal or prismatic directions up to 40% did not give rise to any magnetic moment. DFT calculations showed, additionally, that no magnetic moments were originated either by an isotropic lattice expansion of up to 40%, by the introduction of dilute vacancies or substitutional Fe atoms, or by the presence of stacking faults, as found earlier in palladium [42]. An estimate of the order of magnitude of the volume fraction of the ferromagnetic phase can be obtained as follows: taking into account that the atomic mass of Hf is 178.49 and its density 13310 Kg/m^3, if every Hf atom had a magnetic moment of 0.4 Bohr magnetons (μ_B) (average of the magnetization values corresponding to the stretched monoclinic lattices according to Fig. 5), the total magnetization of the sample would amount to 44.3·KA/m. Fig. 4 reveals that the ferromagnetic component of the sample with the smaller strain (ε~3) is approximately 0.199 KA/m. Thus, the volume fraction with ferromagnetic behavior in this sample would be approximately 0.5%. In the specimen deformed up to a higher strain (ε~8) the corresponding volume fraction would be approximately 0.2%.

The DOS corresponding to the original hcp lattice and to the 20% stretch monoclinic configuration are illustrated in Fig. 6. It can be seen that the break in the symmetry caused by stretching along <101> directions induces a shift of the electronic structure peaks. At stretch values higher than approximately 20% the DOS intensity at the Fermi level is high enough for the system to enhance its stability through the imbalance in the spin occupation, in agreement with the Stoner criterion [5,6]. Conversely, at stretch values higher than 30% the $JN(E_F)$ product sharply decreases, turning the system non-spin polarized.

Fig. 7 shows an enlarged view of the SAED patterns corresponding to the areas illustrated in Figs. 2b (Fig. 7a) and 3a (Fig. 7c), as well as the corresponding radial intensity profiles (Figs. 7b and 7d), calculated adding up the intensity values of each ring of radius r. It can be seen that the SAED pattern of a relatively thick area (Fig. 7b), which includes a number of comparatively large grains (20 nm< d < 50 nm), is mainly formed by rings that match the typical reflections of hcp pure Hf. However, in the SAED pattern corresponding to the rim of the TEM specimen (Fig. 7d), which comprises mostly very fine crystallites (d<20 nm), the radial intensity profile is formed by a very wide peak, encompassing significantly smaller r values than those corresponding to pure hcp Hf, as well as several minor peaks. The reflections corresponding to the magnetic monoclinic lattices that have been predicted to develop with 20% and 29% stretching (Fig. 5) by our DFT calculations, have been superimposed in Fig. 7d. It can be clearly seen that the wide peak appearing in the strained pure Hf can be clearly a result of the superposition of the reflections corresponding to several families of planes of the mentioned magnetic monoclinic lattices.

The excellent match between the measured SAED intensity profile of the nanocrystalline structure and the theoretical reflections of the magnetic monoclinic lattices predicted by DFT, together with the experimentally observed bulk RT ferromagnetic behavior in the strained pure Hf, provide conclusive evidence of the discovery of a new ferromagnetic monoclinic phase. Furthermore, the DFT calculations described above demonstrate the dramatic dependence of the magnetic properties of the monoclinic phase with the stretching direction. Thus, the corresponding magnetic moments will exhibit large anisotropy with well-defined preferential orientations. In these conditions of very large anisotropy, even if the volume fraction of the monoclinic phase is small, i.e., even if a small number of atoms are coupled by exchange interactions, it is possible to observe ferromagnetic behavior instead of superparamagnetism at RT [43].

Annealing the strained pure Hf nanostructures leads to significant grain growth and, simultaneously, to the disappearance of the ferromagnetic component. Fig. 8 compares the RT magnetic response of the initial hcp pure Hf with the response of the samples deformed up to strains of 8, and with that of samples deformed up to strains of 3 and 8 and subsequently heat treated at 1273 K for 5 h. Annealed samples exhibited coarse microstructures, formed by equiaxed grains with average sizes of 30 and 40 μm, respectively (Fig. 8a). Based on the arguments put forward above, it seems logical that lattice recovery during annealing is accompanied by the disappearance of the spontaneous magnetization at RT.

3.1 Outlook

This study provides evidence that nanocrystallization by severe plastic deformation leads to the development of an inhomogeneous distribution of elastic strains, which result in wide variations of the lattice parameters and, thus, of the magnetic character of pure Hf. This constitutes an unprecedented manifestation of the enormous potential of elastic strain engineering to tune the functional properties of materials.

Furthermore, this work highlights the possibility of instilling such elastic strain fields in bulk metals of large dimensions by severe plastic deformation. Controlling the processing parameters such as, in the case of HPT, the applied pressure and the number of turns, will likely allow altering the elastic strain field. It is foreseen that this might be a useful tool to tailor the properties of other metals with high melting points, in which recovery at low temperatures is severely limited and which, therefore, are capable of undergoing nanocrystallization to extremely fine grain sizes.

4. Conclusions

In this work the magnetic behaviour of pure Hf processed at room temperature by high pressure torsion to very high strains is compared to that of the unstrained material. A combined approach, including density functional theory calculations and transmission electron microscopy, is put in place in order to elucidate the origin of the observed changes in the magnetic behaviour with straining. The following conclusions might be drawn from the current study:

1. Severe straining of coarse-grained pure Hf, a classic paramagnet, at room temperature, leads to the development of a nanocrystalline structure with grain sizes ranging from 5 to 50 nm. This nanostructure exhibits room temperature ferromagnetic behaviour.
2. A new monoclinic pure Hf phase forms in the severely strained nanocrystalline structure as a consequence of the elastic lattice distortions triggered by the need to accommodate the imposed strain among neighbouring grains.
3. DFT calculations demonstrate that stretching of the original pure Hf hcp lattice along pyramidal directions up to strains ranging between 15 and 30% leads to a transition to the observed monoclinic lattice, which is endowed with a spontaneous magnetization.
4. Severe plastic deformation might constitute an effective tool to introduce a distribution of elastic strains in high melting point metals and, thus, might allow altering their functional properties to a measurable extent. We expect this approach can be extended to a large number of metals and alloys, thus widening their possibilities for application to yet unexplored limits.

References

1. O. Gutfleisch, M.A. Willard, E. Brück, C.H. Chen, S.G. Sankar, J.P. Liu, Magnetic materials and devices for the 21st century: Stronger, lighter, and more energy efficient, Adv. Mater. 23 (2011) 821-842.

2. E. C. Proc, Collective electron ferromagnetism, R. Soc. London Ser. A 165 (1938) 372-414.
3. E. C. Stoner, E. C. Proc, Collective Electron Ferromagnetism. II. Energy and Specific Heat, R. Soc. London Ser. A 169 (1939) 339-371.
4. G. Urbain, P. Weiss, F. Trombe, Un nouveau métal ferromagnétique, le gadolinium, Comptes Rendus 200, (1935) 2132-2134.
5. W. Heisenberg, Zur Theorie des Ferromagnetismus, Z. Phys. 49, (1928) 619-636.
6. B. D. Cullity, *Introduction to magnetic materials* (Addison-Wesley Publishing Company, 1972).
7. B. Sampedro, P. Crespo, A. Hernando, R. Litrán, J.C. Sánchez-López, C. López-Cartes, A. Fernández, J. Ramírez, J. González-Calbet, M. Vallet, Ferromagnetism in fee Twinned 2.4 nm Size Pd Nanoparticles, Phys. Rev. Lett. 91, (2003) 237203.
8. P. Crespo, R. Litran, T.C. Rojas, M. Multigner, J.M. de la Fuente, J.C. Sánchez-López, M.A. García, A. Hernando, S. Penadés, A. Fernández. Phys. Rev. Lett. 93, 08724 (2004).
9. F. Al Ma'Mari1, T. Moorsom, G. Teobaldi, W. Deacon, T. Prokscha, H. Luetkens, S. Lee, G. E. Sterbinsky, D. A. Arena, D. A. MacLaren, M. Flokstra, M. Ali1, M. C. Wheeler, G. Burnell, B. J. Hickey & O. Cespedes, Beating the Stoner criterion using molecular interfaces, Nature 524 (2015) 69-74.
10. C.M. Cepeda-Jiménez, A. Hernando, J.M. Barandiarán, M.T. Pérez-Prado, Onset of room temperature ferromagnetism by plastic deformation in three paramagnetic pure metals, Scripta Mater. 118 (2016) 41-45.
11. J. Li, Z. Shan, E. Ma, Elastic strain engineering for unprecedented materials properties, MRS Bulletin, 39 (2014) 108-114.

12. J. Feng, X. Qian, C.-W. Huang and J. Li, Strain-engineered artificial atom as a broad-spectrum solar energy funnel, Nature Photonics, 6 (2012) 866-872.
13. H. Li, A. W. Contryman, X. Qian, S. Moeini Ardakani, Y. Gong, X. Wang, J. M. Weisse, C. H. Lee, J. Zhao, P. M. Ajayan, J. Li, H. C. Manoharan, X. Zheng, Optoelectronic crystal of artificial atoms in strain-textured molybdenum disulphide, Nature Comms. 6 (2015) 7381.
14. J. Qi, X. Qian, L. Qi, J. Feng, D. Shi, and J. Li, Strain-engineering of band gaps in piezoelectric boron nitride nanoribbons, Nano Letters 12 (2012) 1224-1228.
15. D. G. Schlom , L.-Q. Chen , C. J. Fennie , V. Gopalan , D. A. Muller , X. Pan, R. Ramesh , R. Uecker, Elastic strain engineering of ferroic oxides, MRS Bulletin 39 (2014) 118-130.
16. S.E. Thomson , M. Armstrong, C. Auth , M. Alavi , M. Buehler et al., A logic nanotechnology featuring strained-silicon, IEEE Trans. Electron Devices 51 (2004) 1790-1793.
17. B. Yildiz, Stretching the energy landscape of oxides - Effects on electrocatalysis and diffusion, MRS Bulletin 39 (2014) 147-156.
18. D. Yu, J. Feng, J. Hone, Elastically strained nanowires and atomic sheets, MRS Bulletin 39 (2014) 157-162.
19. S. Hao, L. Cui, H.Wang, D. Jiang, Y. Liu, J. Yan, Y. Ren, X. Han, D. E. Brown, J. Li, Retaining large and adjustable elastic strains of kilogram-scale Nb nanowires, ACS Applied Materials & Interfaces 8 (2016) 2917-2922.
20. T.B. Massalski, Binary Alloy Phase Diagrams, ASM International, Materials Park, OH, 1990.

21. High pressure phase transformations: a handbook, E. Yu. Tonkov, Routledge, 1992.

22. U.M.R. Seelam, C. Suryanarayana, Mechanically induced fcc phase formation in nanocrystalline hafnium, J. Appl. Phys. 105 (2009) 063524.

23. A.P. Zhilyaev, T.G. Langdon, Using high-pressure torsion for metal processing: Fundamentals and applications, Prog. Mater. Sci. 53 (2008) 893-979.

24. J.P. Perdew, K. Burke, M. Ernzerhof, Generalized gradient approximation made simple, Phys. Rev. Lett. 77 (1996) 3865-3868.

25. G. Kresse, D. Joubert, From ultrasoft pseudopotentials to the projector augmented-wave method, Phys. Rev. B 59 (1999) 1758-1775.

26. G. Kresse, J. Hafner, Ab initio molecular dynamics for liquid metals, Phys.Rev. B 47 (1993) 558-561.

27. G. Kresse, J. Furthmüller, Efficient iterative schemes for ab initio total-energy calculations using a plane-wave basis set, Phys. Rev. B 54, (1996) 11169-11186.

28. R.W.G. Wyckoff, in *Crystal Structures* (Second edition, Interscience Publishers, New York. 1963) vol. 1, p.77.

29. H. J. Monkhorst, J. D. Pack, Special points for Brillouin-zone integrations, Phys. Rev. B 13 (1976) 5188-5192.

30. J. M Soler, E. Artacho, J. D. Gale, A. García, J. Junquera, P. Ordejón, D. Sánchez-Portal, The SIESTA method for ab initio order-N materials simulation, J. Phys. Cond. Matt. 14 (2002) 2745-2779.

31. K. Edalati, Z. Horita, Y. Mine, High pressure torsion of Hf, Materials Science and Engineering 527 (2010) 2136-2141

32. H. Gleiter, Nanostructured materials: basic concepts and microstructure, Acta Mater. 48 (2000) 1-29.
33. G. Palumbo, S.J. Thorpe, K.T. Aust, On the contribution of triple junctions to the structure and properties of nanocrystalline materials, Scripta Metall. 24 (1990) 1347-1350.
34. L. Lu, M. L. Sui, K. Lu, Superplastic extensibility of nanocrystalline copper at room temperature, Science 287 (2000) 1463-1466.
35. L. Lu, Y. Shen, X. Chen, L. Qian, K. Lu, Ultrahigh strength and high electrical conductivity in copper, Science 304 (2004) 422-426.
36. Y. Wang, M. Chen, F. Zhou, E. Ma, High tensile ductility in a nanostructured metal, Nature 419 (2002) 912-915.
37. D. B. Witkin, E. J. Lavernia, Synthesis and mechanical behavior of nanostructured Materials via cryomilling, Prog. Mater. Sci. 51 (2006) 1-60.
38. B. Poudel, Q. Hao, Y. Ma, Y. Lan, A. Minnich, B. Yu, X. Yan, D. Wang, A. Muto, D. Vashaee, X. Chen, J. Liu, M.S. Dresselhaus, G. Chen, Z. Ren, High-thermoelectric performance of nanostructured bismuth antimony telluride bulk alloys, Science 320 (2008) 634-638.
39. Y.B. Guo, T.Xu, M. Li, Atomistic calculation of residual stress in nanoscale polycrystalline materials, Phil. Mag. 92 (2012) 3064-3083.
40. G.K. Rane, U.Welzel, S.R. Meka, E.J. Mittemeijer, Non-monotonic lattice parameter variation with crystallite size in nanocrystalline solids, Acta mater. 61 (2013) 4524-4533.
41. K.S. Kumar, H. Van Swygenhoven, S. Suresh, Mechanical behavior of nanocrystalline metals and alloys, Acta mater. 51 (2003) 5743-5774.

42. S. S. Alexandre, M. Mattesini, J.M. Soler, F. Ynduráin, Magnetism of two-dimensional defects in Pd: Stacking faults, twin boundaries, and surfaces, Phys. Rev. B. 74 (2006) 054405.
43. P. Gambardella, S. Rusponi, M. Veronese, S. S. Dhesi, C. Grazioli, A. Dallmeyer, I. Cabria, R. Zeller, P. H. Dederichs, K. Kern, C. Carbone, H. Brune, Giant magnetic anisotropy of single cobalt atoms and nanoparticles, Science 300 (2003) 1130-1133.

Figure captions

Figure 1. Microstructure of the as-received pure Hf. (a) SEM micrograph showing the coarse-grained, equiaxed polycrystalline structure; (b) TEM micrograph illustrating the presence of a small dislocation density within the grain interiors.

Figure 2. Nanostructure of pure Hf severely deformed by high pressure torsion up to a strain of (a) ε~3 and (b) ε~8. TEM bright field images and the corresponding SAED pattern.

Figure 3. (a) STEM image and SAED pattern of a very thin region located at the rim of the specimen; (b) high resolution STEM image of very thin region located at the rim of the specimen.

Figure 4. Magnetic response of as-received and severely strained pure Hf. (a) Comparison of the RT magnetization curves corresponding to the as received material and to samples severely deformed up to ε~3 and ε~8; (b) Thermal dependence of the magnetization (H_{appl}=1 T) for the as-received pure Hf and for a sample severely deformed up to ε~8.

Figure 5. DFT calculations of the evolution of the total magnetic moment with stretching along selected crystallographic directions. The crystal lattices corresponding to the original hcp lattice as well as to the 20% and 29% stretch configurations are overlaid in the same graph.

Figure 6. DOS corresponding to the unstrained pure Hf and to the 20% stretch configuration along the <101> direction. Note the relative shift between spin up and down DOS maxima near the Fermi level (E_f).

Figure 7. TEM analysis of the nanocrystalline structure developed upon severe plastic deformation processing of pure Hf. (a) SAED pattern of the region imaged in Fig. 2b and (b) the corresponding radial intensity profile. Red lines indicate the r-values corresponding to several (hkl) planes of the original Hf hcp lattice; (c) SAED pattern of the region imaged in Fig. 3a and (d) the corresponding radial intensity profile. Red lines indicate the r-values corresponding to several (hkl) planes of the original Hf hcp lattice; blue and green lines indicate (hkl) planes corresponding to the monoclinic lattices developed following, respectively, 20% and 29% stretch along the <101> directions, as predicted by DFT calculations.

Figure 8. (a) Microstructure of the pure Hf deformed up to a strain of ε~8 and, subsequently, annealed at 1273 K for 5 h. (b) Reduction of the RT ferromagnetic component by annealing**.** Comparison of the RT magnetization curves corresponding to the as received pure Hf (solid dark line), to a sample deformed up to a strain of ε~8 (dotted line) and, to samples deformed up to strains of ε~3 and ε~8 and, subsequently, annealed at 1273 K for 5 h (red and blue solid lines, respectively).

Acknowledgments

I. Orúe, P. Marín and A. Aragón are sincerely appreciated for their help with the magnetic measurements. We are thankful to the staff at the CAI Técnicas Geológicas of the Complutense University for their assistance with the chemical analysis by ICP-OES. Dr. A. Zhilyaev acknowledges a TECNIOSPRING grant financed by Generalitat de Catalunya and co-funded by the 7th Framework programme of the EU. The research leading to these results has received funding from the European Commission (ExoMet Project, 7th Framework Programme, contract FP7-NMP3-LA-2012-280421), from the Madrid region under programmes S2013/MIT-2775 (DIMMAT-CM) and S2013/MIT-2850 (NANOFRONTMAG-CM), as well as from Spanish MINECO (Ministerio de Economía y Competitividad) (MAT2012-37109-C02-01 and MAT2013-48009-C4-1). JIB thankfully acknowledges the computer resources, technical expertise and assistance provided by the Spanish Supercomputing Network (RES) and CeSViMa.

	Ca	**K**	**P**	**S**	**Pd**	**W**	**Zr**	**Ag**	**Pt**	**Fe**	**Hf**
As-received	-	-	-	67	75	1585	1187	19	16	142	Bal.
$\varepsilon \sim 8$	17	208	178	47	90	1647	1234	32	8	207	Bal.

Table 1. Chemical composition (ppm) of the pure Hf in the as-received state and after HPT processing using 6 GPa and N=5 at RT up to strains of $\varepsilon \sim 8$.

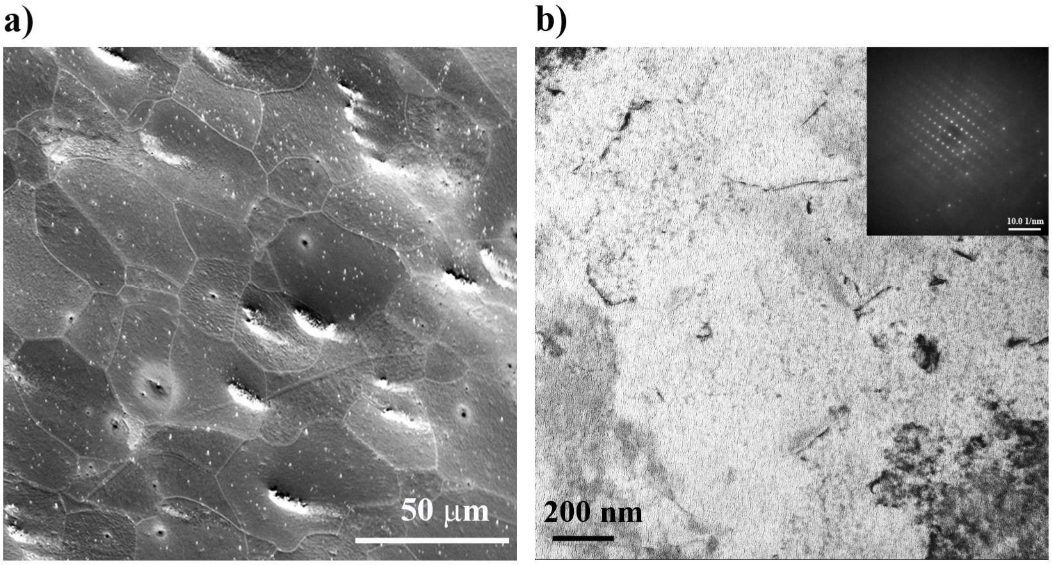
a)
b)
50 μm
200 nm
10.0 1/nm

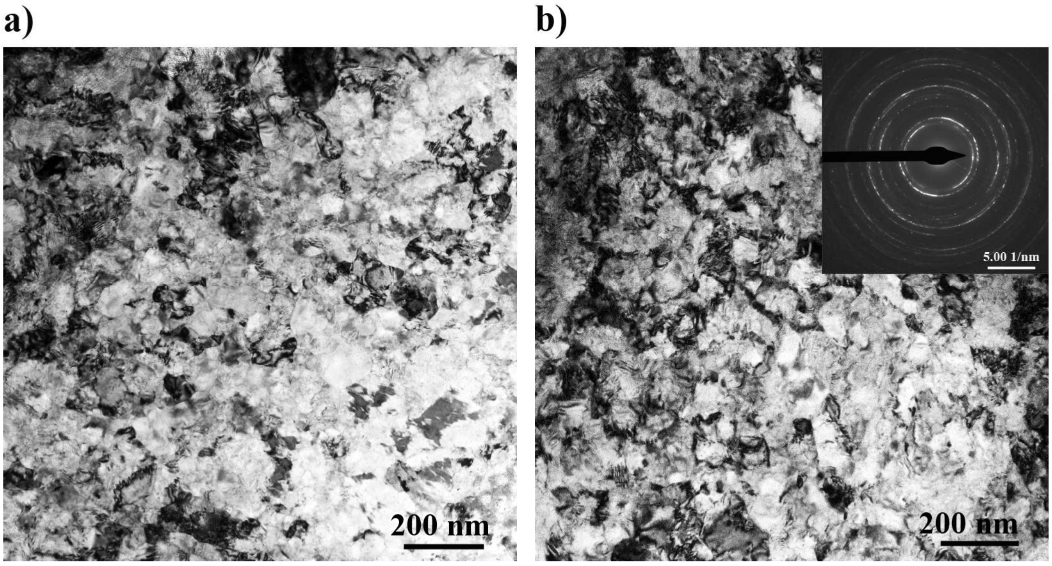
a)
b)
5.00 1/nm
200 nm
200 nm

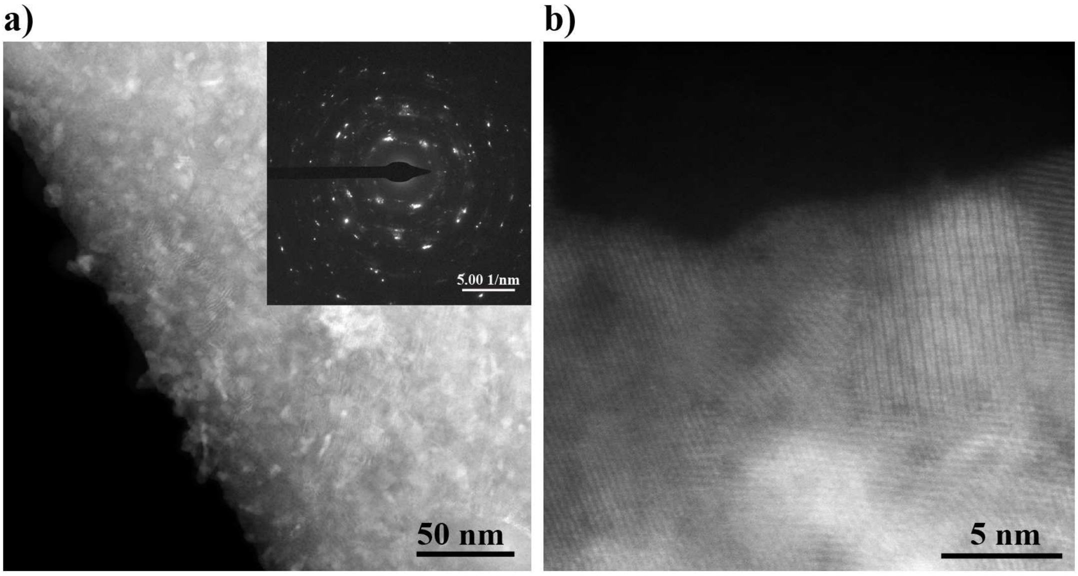
a)
5.00 1/nm
50 nm
b)
5 nm

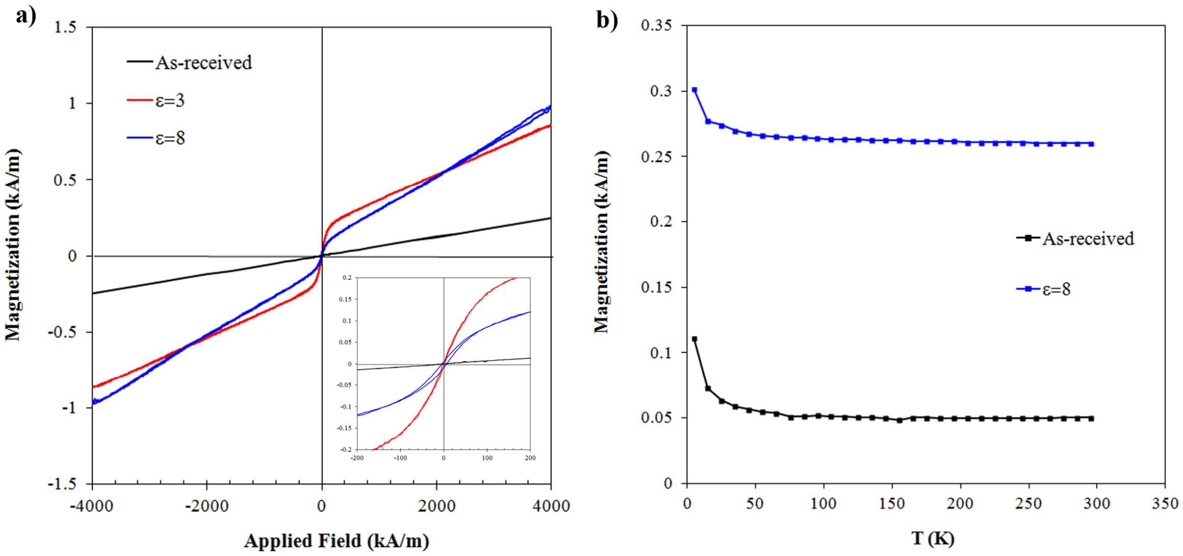
a)
Magnetization (kA/m)
Applied Field (kA/m)
As-received
ε=3
ε=8
1.5
1
0.5
0
-0.5
-1
-1.5
-4000
-2000
0
2000
4000
b)
Magnetization (kA/m)
T (K)
As-received
ε=8
0.35
0.3
0.25
0.2
0.15
0.1
0.05
0
0
50
100
150
200
250
300
350

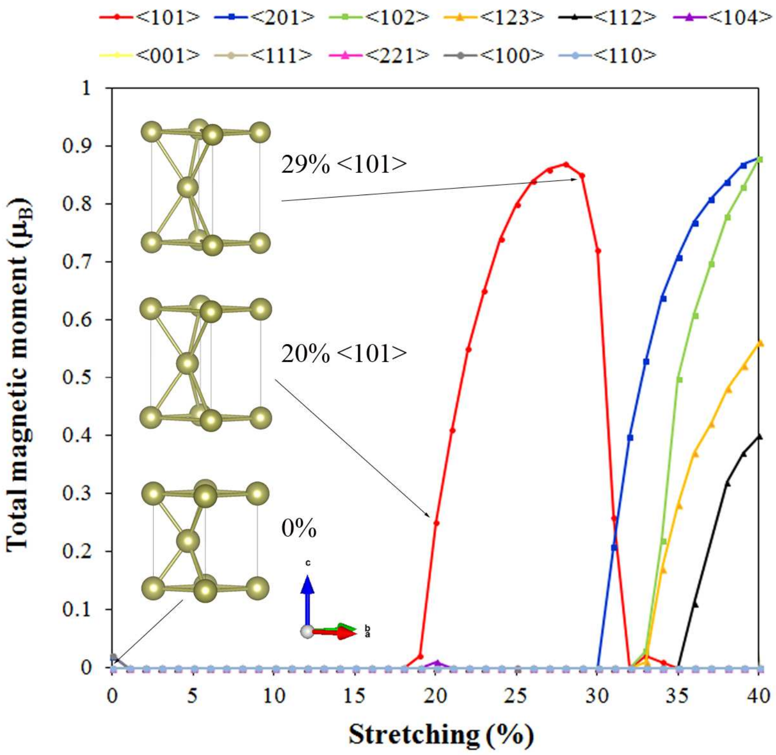

<101>
<201>
<102>
<123>
<112>
<104>
<001>
<111>
<221>
<100>
<110>
Total magnetic moment (μ_B)
Stretching (%)
29% <101>
20% <101>
0%
c
b
a
0
0.1
0.2
0.3
0.4
0.5
0.6
0.7
0.8
0.9
1
0
5
10
15
20
25
30
35
40

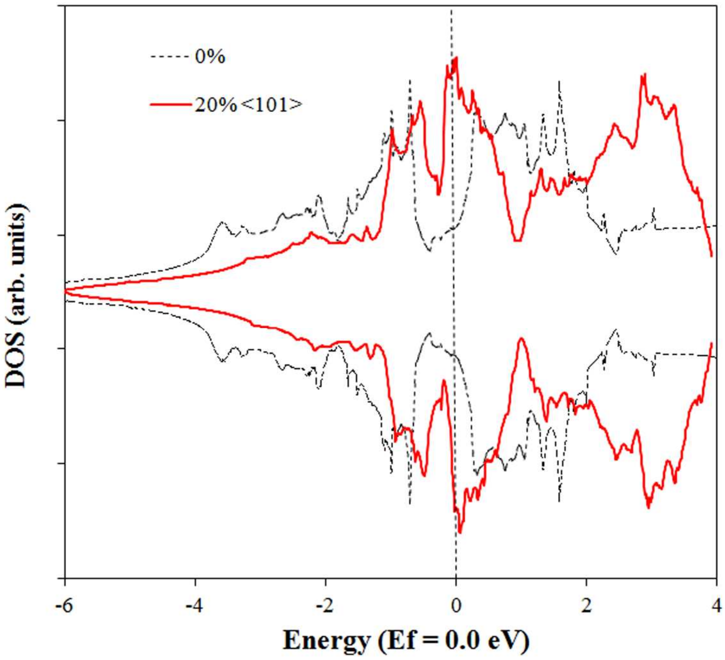
0%
20% <101>
DOS (arb. units)
-6
-4
-2
0
2
4
Energy (Ef = 0.0 eV)

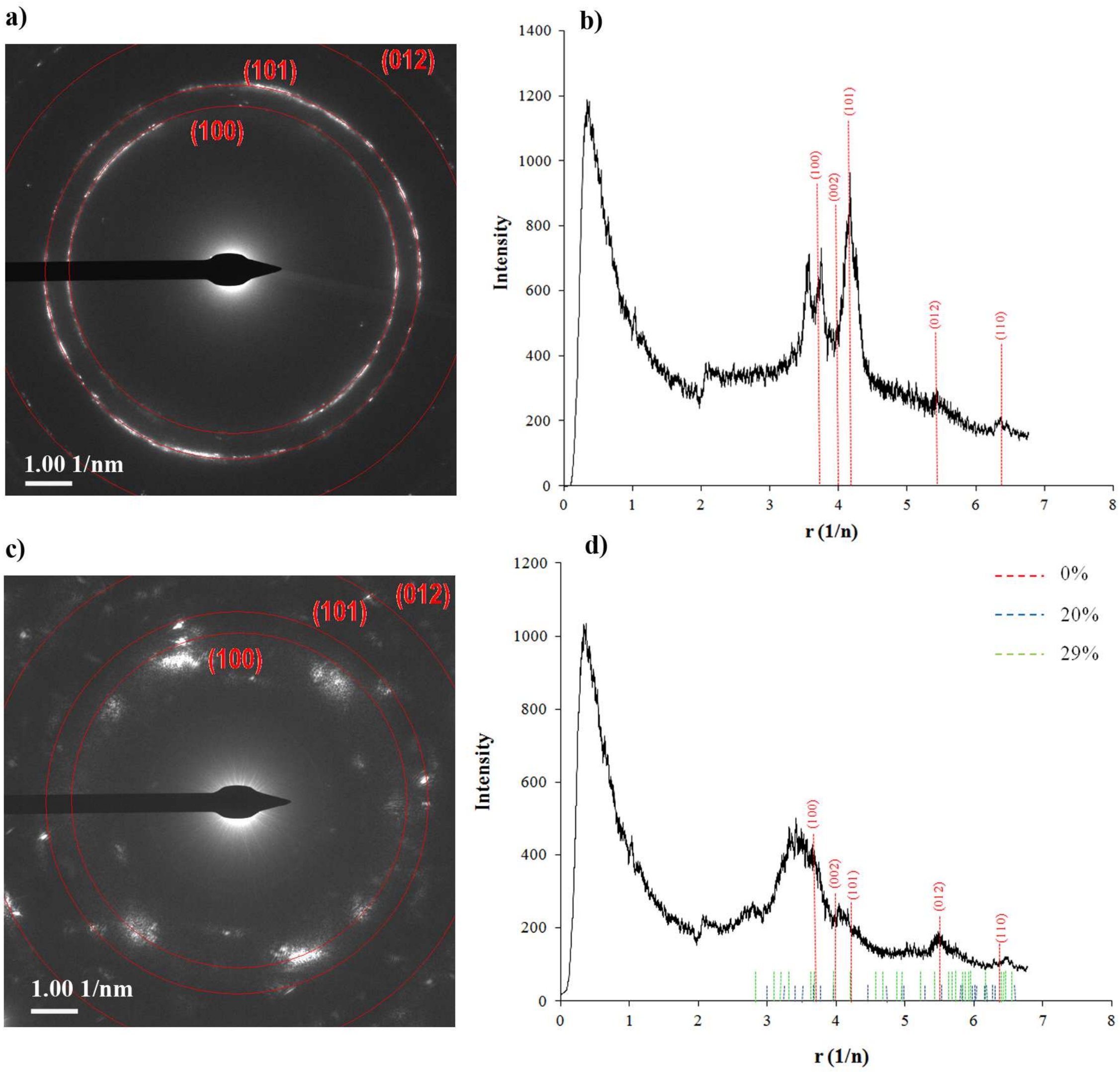
a)
(101)
(012)
(100)
1.00 1/nm
b)
1400
1200
1000
800
600
400
200
0
Intensity
(100)
(002)
(101)
(012)
(110)
0 1 2 3 4 5 6 7 8
r (1/n)
c)
(101)
(012)
(100)
1.00 1/nm
d)
1200
1000
800
600
400
200
0
Intensity
0%
20%
29%
(100)
(002)
(101)
(012)
(110)
0 1 2 3 4 5 6 7 8
r (1/n)

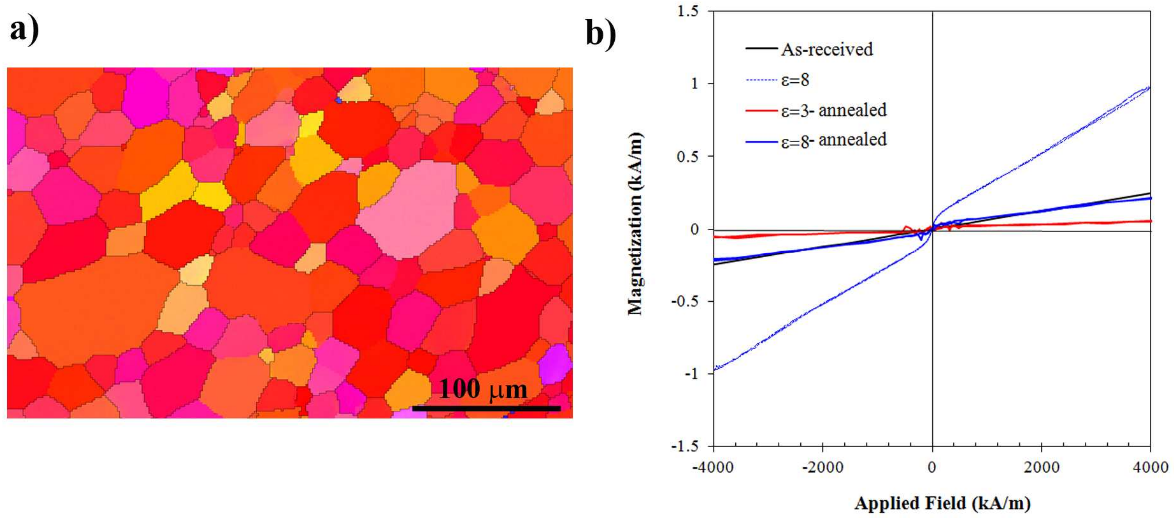
a)
100 μm
b)
As-received
ε=8
ε=3- annealed
ε=8- annealed
Magnetization (kA/m)
1.5
1
0.5
0
-0.5
-1
-1.5
-4000
-2000
0
2000
4000
Applied Field (kA/m)